Numazawa et al. *NPG Asia Materials* (2018) 10: 397–405
DOI 10.1038/s41427-018-0045-2

NPG Asia Materials

ARTICLE Open Access

Multistage redox reactions of conductive-polymer nanostructures with lithium ions: potential for high-performance organic anodes

Hiromichi Numazawa[1], Kosuke Sato[1], Hiroaki Imai[1] and Yuya Oaki[1]

Abstract

Conducive polymers have a wide range of applications originating from their π-conjugated systems. The redox reactions of conductive polymers with doping and dedoping of anions have been applied to cathodes for charge storage. In contrast, the redox reactions with cations have not been fully studied in anodes for charge storage. Here, we found that the nanostructures of conductive polymers, such as polypyrrole (PPy) and polythiophene (PTp) derivatives, have reversible redox reactions with cations. The PPy and PTp nanostructures acted as anodes with specific capacities of 157 and 44.4 mA h g^{-1}, respectively, at a current density of 20 mA g^{-1}. The introduction of a carboxy group to the pyrrole and thiophene rings enhanced the specific capacities up to 730 and 963 mAh g^{-1}, respectively. The enhanced electrochemical properties were not observed in the bulk-size conductive polymers. The results suggest that conductive-polymer nanostructures have potential for developing metal-free, high-performance charge storage devices.

Introduction

Conductive polymers have electrochemical, electronic, and photochemical properties originating from their π-conjugated system[1–21]. The electrochemical redox reactions with doping and dedoping of anions (p doping) have been studied for charge storage applications (Fig. 1a), such as aqueous redox capacitors and lithium-ion batteries[13–21]. The theoretical capacity is determined by the doping level, such as 136 mAh g^{-1} for polypyrrole (PPy) with a maximum 33 mol% anion doping and 82 mAh g^{-1} for polythiophene (PTp) with 25 mol% anion doping[13,16,19,21]. The improved electrochemical properties were achieved by the design of the molecules and morphologies[17,21–28]. Our group reported new methods for the simultaneous synthesis and morphology control of conductive polymers using solid-state oxidant crystals[24–28]. In contrast, the electrochemical redox reactions of conductive polymers with doping and dedoping of cations (n doping) have not been fully studied for charge storage applications (Fig. 1b). In earlier works[16,29–38], conductive polymers, such as polyacetylene (PA)[29–31], PPy[32], PTp[33–35], and polyacene derivatives[36–38], showed redox reactions with n doping in the potential range of 2.0–0.5 V vs. Li/Li^+. The earlier works concluded that the n-doping reaction is not suitable for the anode-active material in lithium-ion batteries because of the low specific capacity and structure instability[16]. Moreover, the redox reactions of conductive polymers lower than 0.5 V vs. Li/Li^+ were not explored in previous works (Fig. 1c). Here, we found that the reversible multiple redox reactions of conductive polymers, such as PPy and PTp derivatives, proceed with the charge and discharge of Li^+ within 3.0–0.01 V vs. Li/Li^+ (Fig. 1b, c). The introduction of carboxy groups to the pyrrole (Py) and thiophene (Tp) rings induces a drastic increase in the specific capacity. Furthermore, the nanostructures of the

Correspondence: Yuya Oaki (oakiyuya@applc.keio.ac.jp)
[1]Department of Applied Chemistry, Faculty of Science and Technology, Keio University, 3-14-1 Hiyoshi, Kohoku-ku, Yokohama 223-8522, Japan

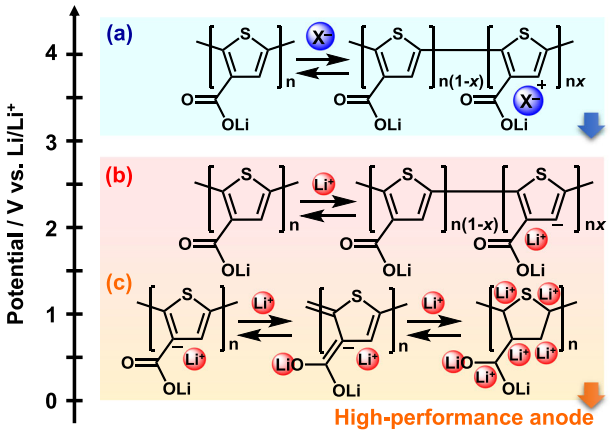

Fig. 1 Electrochemical redox reactions of PTp-COOH. a Redox reaction with doping and dedoping of anions (X^-) (p doping). **b** Redox reaction with doping and dedoping of cations, such as Li^+ (n doping). The neutral state is stable in the white region between panels (**a**) and (**b**) at approximately 3 V. **c** Redox reactions with the charge and discharge of cations in the heteroaromatic ring and carbonyl substituent. The red balls represent the Li^+ electrochemically reacted with the monomer unit during the charge–discharge reactions

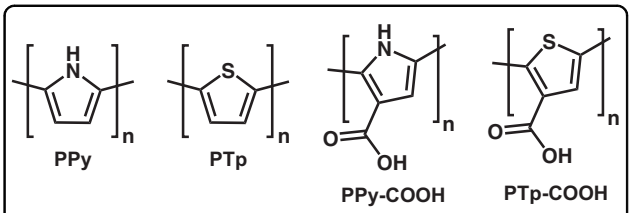

Scheme 1 Molecular structures of PPy, PPy-COOH, PTp, and PTp-COOH

conductive polymers play important roles in the enhanced electrochemical properties. Nanoparticles of PPy and PTp with carboxy groups (PPy-COOH and PTp-COOH) have specific capacities of 730 and 963 mAh g^{-1}, respectively, at 20 mA g^{-1} with stable cycle performances.

In recent years, redox-active organic materials based on π-conjugated molecules have attracted much interest as high-performance anodes for lithium-ion batteries[39–56]. The π-conjugated molecules with carboxy substituents, such as phthalic acid and muconic acid, have a reversible redox reaction based on lithium alkoxylation at approximately 1.0 V vs. Li/Li^+[41,42]. At potentials lower than 1.0 V vs. Li/Li^+, a redox reaction with the charge and discharge of multiple Li^+ ions was reported for a π-conjugated system with carboxy substituents[43–51]. Although a high specific capacity was found with low-molecular-weight compounds (Table S1 in the Supplementary Information)[41–51], their solubility and low conductivity caused problems with the cycle stability. A high specific capacity and cycle stability were achieved with polymer-based anodes, such as polydopamine and heterocyclic ladder polymers (Table S2 in the Supplementary Information)[52–56]. However, the design strategies for the molecules and hierarchical morphologies were not fully studied to achieve further improved properties in polymer-based anodes. Here, we focused on conductive polymers because molecular and morphological designs have been extensively studied in previous works[1–12]. If conductive polymers are used as the anode in lithium-ion batteries, design strategies for the molecules and morphologies can be effectively applied to enhance the electrochemical properties. Here, we found overlooked electrochemical properties of conductive polymers, such as PPy-COOH and PTp-COOH, within 3.0–0.01 V (Scheme 1). Both the molecular structures and nanoscale morphologies influence the electrochemical properties. The conductive-polymer nanostructures showed multistage redox reactions with Li^+ within 3.0–0.01 V vs. Li^+ (Fig. 1b, c). The PTp-COOH nanostructures had the highest specific capacity, namely, 963 mAh g^{-1} at 20 mA g^{-1}, with a high cycle stability and Coulombic efficiency. In contrast, enhanced properties were not observed with the bulk-size conductive polymers. The present study indicates the overlooked potentials of conductive polymers as high-performance organic anodes.

Materials and methods

Synthesis of the conductive-polymer nanostructures

All reagents were used as purchased without purification.

Synthesis of PPy

A monomer solution containing 0.72 mmol of Py (TCI, 99.0%) was prepared with 25 cm^3 of 2-propanol (Kanto, 97%). Then, 2.5 mmol of copper chloride dihydrate ($CuCl_2{\cdot}2H_2O$, Kanto, 99.7%) was added to the monomer solution. When PPy particles with a larger size were synthesized, the same concentration of iron chloride anhydrous ($FeCl_3$, Kanto, 96.0%) was used as the oxidant in chloroform (Kanto, 99.0%). The solutions were stirred at 25 °C for 24 h. The resultant precipitate was filtered, washed with 1.0 mol dm^{-3} hydrochloric acid (HCl) and toluene, and then dried at room temperature.

Synthesis of PPy-COOH

A monomer solution containing 0.5 mmol of pyrrole-3-carboxylic acid (Py-COOH, TCI, 95.0%) was prepared with 15 cm^3 of chloroform (Kanto, 99.7%). Then, 15 cm^3 of a chloroform solution containing 1.0 mmol of $FeCl_3$ was added to the monomer solution. The solution was stirred for 24 h at 25 °C. The resultant precipitate was filtered, washed with 1.0 mol dm^{-3} HCl and toluene, and then dried at room temperature.

Commercial PTp

Commercial PTp (Aldrich, poly(thiophene-2,5-diyl), bromine terminated) was used because the sample had nanostructures.

Synthesis of PTp-COOH

A precursor solution containing 1.2 mmol of thiophene-3-carboxylic acid (Tp-COOH, TCI, 98.0%), 3.6 mmol of ammonium peroxosulfate (APS, Kanto, 98%), and 18 mmol of $FeCl_3$ was prepared with 25 cm^3 of 1.2 mol dm^{-3} HCl. Then, 1.2 mmol of Tp-COOH was added to the HCl solution twice every 30 min. A total of 3.6 mmol of Tp-COOH was used for the polymerization. When PTp-COOH particles with a larger size were synthesized, 15 cm^3 of an HCl solution containing 3.6 mmol of Tp-COOH and 3.6 mmol of APS was mixed with 10 cm^3 of an HCl solution containing 18 mmol of $FeCl_3$. These solutions were stirred for 24 h at 60 °C. The resultant precipitate was filtered, washed with 1.0 mol dm^{-3} HCl and toluene, and then dried at room temperature.

Structure characterization

The structures of the conductive polymers were characterized by Fourier transform infrared (FT-IR) absorption spectroscopy (JASCO, FT/IR-4200) and X-ray photoelectron spectroscopy (XPS) (JEOL, JPS-9010TR). Calibration of the peak position in the XPS profile was performed by the peak of Au $4f_{7/2}$. The powder samples were mixed with potassium bromide (KBr) for the FT-IR analysis. The composition was estimated from the CHN elemental analysis. The remaining metal content was analyzed by thermogravimetry (TG, Seiko, TG/DTA7200) under air conditions. The morphologies of the conductive polymers were observed by field-emission scanning electron microscopy (SEM, Hitachi S-4700, and JEOL JSM7600F) operated at 3.0 or 5.0 kV.

Electrochemical properties

The electrochemical properties were measured using a three-electrode setup in a twin-beaker cell. The working electrode was prepared by mixing 60 wt% conductive polymer as the active material, 30 wt% acetylene black as a conductive carbon, and 10 wt% poly(vinylidene fluoride) (PVDF) as the binder. The weight of the active material was approximately 1 mg. A slurry of these materials with a small amount of *N*-methyl-2-pyrrolidone (Junsei Chemical, 99%) was dropped on a copper mesh as a current collector. The counter and reference electrodes were composed of lithium metal. The electrolyte was 1 mol dm^{-3} lithium perchlorate ($LiClO_4$) in ethylene carbonate (EC) and diethyl carbonate (DEC) (1/1 by volume). Chronopotentiometry was performed using a charge–discharge measurement system (Hokuto Denko, HJ1001SD8) with a cut-off voltage between 3.0 and 0.01 V vs. Li/Li^+. Cyclic voltammetry (CV) was measured using a potentiostat (Princeton Applied Research, VersaSTAT 3) at a scan rate of 1 mV s^{-1}.

Density functional theory calculations of the energy levels

The energy levels of the unoccupied molecular orbitals were estimated by density functional theory (DFT) calculations using Gaussian software. The structure optimization was performed on tetramers of Py, Py-COOH, Tp, and Tp-COOH. Then, the energy levels were calculated by B3LYP.

Results

Nanostructures of PPy, PTp, PPy-COOH, and PTp-COOH

Nanostructures of four conductive polymers, PPy, PTp, PPy-COOH, and PTp-COOH, were prepared to study their electrochemical properties (Scheme 1). The detailed synthetic procedure and structure characterization are described in the Supplementary Information. The nanostructures of PPy, PPy-COOH, and PTp-COOH were synthesized by chemical oxidative polymerization (Fig. 2). Commercial PTp was used as the nanostructure sample. The characteristic absorption peaks assigned to those polymers were observed in the FT-IR spectra (Fig. 2a and the Supplementary Information). The detailed peak assignments are described in the Supplementary Information. The CHNS elemental analysis supported the formation of conductive polymers even though some non-conjugated part was included (Table S3 in the Supplementary Information). The formation of these conductive polymers was also supported by the XPS results (Figure S1 in the Supplementary Information). The weight percent of the remaining species was estimated to be less than 0.09% for PTp-COOH from the TG analysis. The remaining species were not detected for PPy, PPy-COOH, and PTp after heating them up to 1000 °C by TG analysis (Figure S2 in the Supplementary Information). In addition, trace metals originating from the oxidative agents were not detected in the XPS analysis (Figure S1 in the Supplementary Information). All of the polymers showed nanostructures approximately 200 nm in size (Fig. 2b–e). PPy, PPy-COOH, and PTp-COOH had nanoparticles 311 ± 81, 177 ± 53, and 165 ± 41 nm in diameter, respectively (Fig. 2b, c, e). Nanoflakes approximately 300 nm in size were observed for the aggregate of commercial PTp (Fig. 2d).

Electrochemical properties of PPy, PTp, PPy-COOH, and PTp-COOH nanostructures with Li^+

The PPy, PPy-COOH, PTp, and PTp-COOH nanostructures showed charge–discharge reactions with Li^+ in the potential range of 3.0–0.01 V vs. Li/Li^+ at 20 mA g^{-1} (Fig. 3a, c). CV was performed on these polymer nanostructures at 1 mV s^{-1} (Fig. 3b, d). The electrochemical

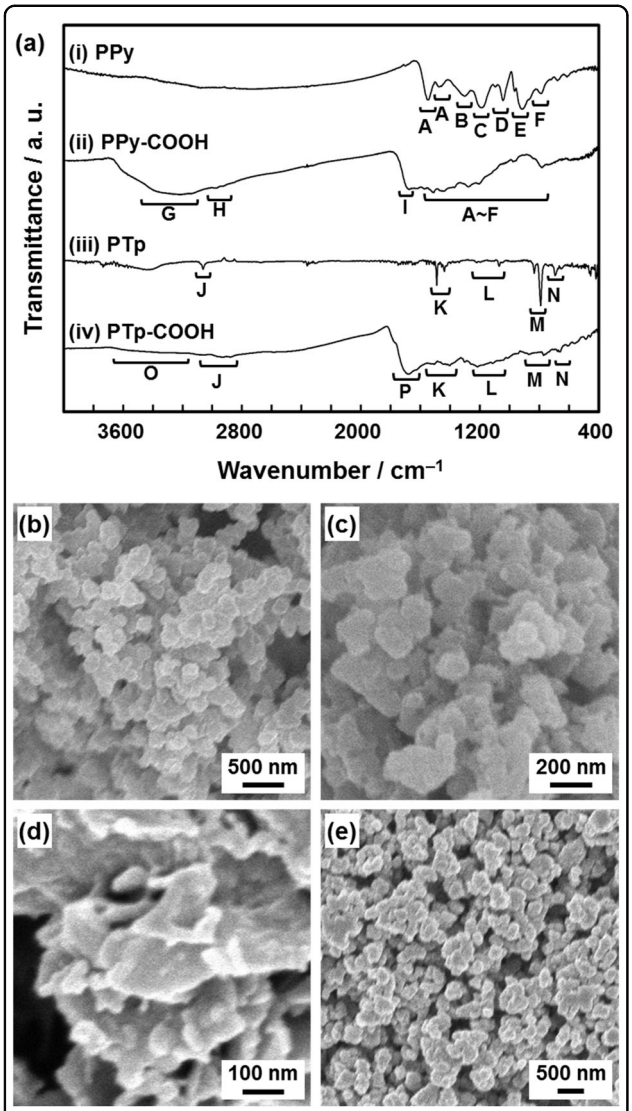

Fig. 2 PPy, PPy-COOH, PTp, and PTp-COOH nanostructures. a FT-IR spectra of PPy (i), PPy-COOH (ii), PTp (iii), and PTp-COOH (iv). The detailed peak assignments are described in the Supplementary Information. **b–e** Scanning electron microscopy (SEM) images of the PPy (**b**), PPy-COOH (**c**), PTp (**d**), and PTp-COOH (**e**) nanostructures

properties of these polymers were measured in EC/DEC (1/1 by volume) containing 1 mol dm^{-3} $LiClO_4$ using a three-electrode setup in a twin-beaker cell. The working electrode was prepared by mixing 60 wt% conductive polymer as the active material, 30 wt% acetylene black as a conductive carbon, and 10 wt% PVDF as the binder. The molar ratio of the electrochemically incorporated Li^+ to the monomer unit (x) in the redox reaction was estimated from the specific capacity of the second discharge cycle (Fig. 3 and Table 1) because the first cycle included the irreversible capacity corresponding to formation of the solid electrolyte interphase (Figure S3 in the Supplementary Information). Although the proton of the carboxy group exchanges with Li^+ by ion exchange in the electrolyte solution and/or the first reduction reaction, this Li^+ is not counted in the x value. In other words, lithium carboxylate is not included in the calculation of the specific capacity. The discharge curve of the PPy nanoparticles showed a two-step potential change within 3.0–0.01 V vs. Li/Li^+ at 20 mA g^{-1} (Fig. 3a). PPy as an anode had a specific capacity of 157 mAh g^{-1} with $x =$ 0.382 after the contribution of the conductive carbon to the specific capacity was subtracted (Figure S4 in the Supplementary Information). The specific capacity and x, except the charge–discharge curve, are shown in the present report after the capacity resulting from the carbon was subtracted (Table 1). The specific capacity drastically increased up to 730 mAh g^{-1} with $x = 3.03$ for the PPy-COOH nanoparticles (Fig. 3a and Table 1), although PPy-COOH showed a two-step potential change similar to that of PPy. The CV curves showed the current corresponding to the redox reactions of the PPy and PPy-COOH nanostructures in the same potential range as that observed in the charge–discharge curves (Fig. 3b). The introduction of a carboxy group induced a drastic increase in the specific capacity. The electrochemical properties of the PTp and PTp-COOH nanostructures were similar to those of the PPy and PPy-COOH nanostructures (Fig. 3c, d and Table 1). PTp and PTp-COOH showed specific capacities of 44.4 mAh g^{-1} with $x = 0.136$ and 963 mAh g^{-1} with $x = 4.53$, respectively. As studied in previous works[16,32–35], the electrochemical properties of PPy and PTp were not as high. In contrast, the introduction of carboxy groups to the Py and Tp rings plays an important role in the drastic increase in the x and specific capacity (Table 1). In the electrochemical characterization, the x values in the charge–discharge reaction were reproducible for the same types of conductive polymers (Table S4 in the Supplementary Information).

Cycle stability, rate performance, and particle-size effect

The cycle stability, rate performance, and particle-size effect were studied for PPy and PTp-COOH (Fig. 4 and Figure S5 in the Supplementary Information). A reversible charge–discharge reaction was observed for the PTp-COOH nanostructure at a higher current density (Fig. 4a). However, the specific capacity of PPy was low (Figure S5 in the Supplementary Information). The specific capacity of the PTp-COOH nanoparticles was 190 mAh g^{-1} at 500 mA g^{-1} (Fig. 4a) and was reproducible (Figure S6 in the Supplementary Information). Particles with larger sizes, such as 7 μm for PPy and 1 μm for PTp-COOH, were prepared by changing the synthetic conditions (Figure S7 in the Supplementary Information). The specific capacity of the PTp-COOH particles with a larger size decreased for all current densities (Fig. 4a). The same trend was observed for the PPy particles, even though the

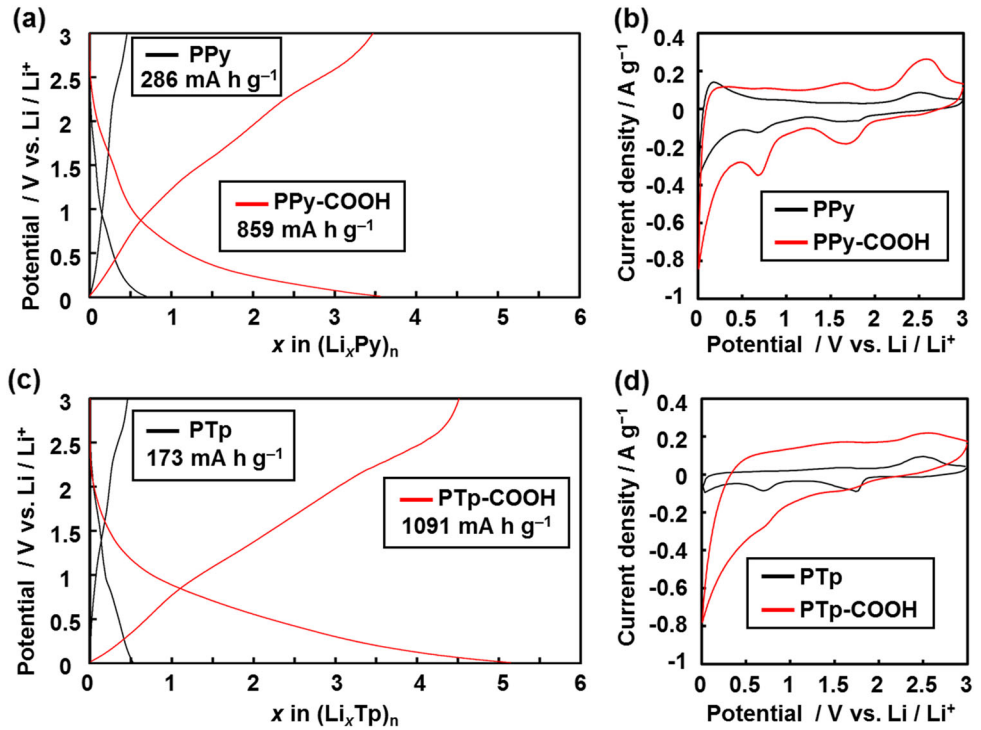

Fig. 3 Charge–discharge (**a**, **c**) and CV (**b**, **d**) curves of the PPy, PPy-COOH (**a**, **b**), PTp, and PTp-COOH (**c**, **d**) nanostructures from the second cycle. The current density was 20 mA g^{-1} for the charge–discharge measurements. The scan rate was 1 mV s^{-1} on the CV curves. The charge–discharge curves of the first cycle and the reproducibility of the *x* values are shown in Figure S3 and Table S4 in the Supplementary Information

Table 1 Specific capacity and molar ratio of Li^+ electrochemically reacted with the monomer unit (*x*) at 20 mA g^{-1}

Samples	[a]Observed values		[b]Corrected values	
	Specific capacity (mAh g^{-1})	[c]*x* /– (3.0–0.01 V vs. Li/Li+)	Specific capacity (mAh g^{-1})	[c]*x* /– (3.0–0.01 V vs. Li/Li+)
PPy	286	0.694	157	0.382
PPy-COOH	859	3.56	730	3.03
PTp	173	0.529	44.4	0.136
PTp-COOH	1091	5.38	963	4.53

[a] These values are data from the charge–discharge curves without any correction
[b] Since conductive carbon has a specific capacity in the electrode, the specific capacity was subtracted from the observed values by the method shown in Figure S4 in the Supplementary Information
[c] The *x* value was defined as the molar ratio of the electrochemically incorporated Li^+ to the monomer unit (*x*) in the redox reaction
This means that Li^+ on the carboxylate group was not counted in the *x* value

specific capacity was low (Figure S7 in the Supplementary Information). Since the diffusion distance of Li^+ is shortened by the decrease in the particle size, a higher specific capacity is achieved with the nanoparticles. After 1000 cycles, the PTp-COOH nanoparticles showed specific capacities of 147 mAh g^{-1} and 98.5% of the Columbic efficiency at 500 mA g^{-1} (Fig. 4b). The specific capacity varied within approximately 20% during 1000 cycles. Since a large volume change with the incorporation of multiple Li^+ ions occurs in the PTp-COOH nanoparticles, the specific capacity has slight variations during cycling. The results indicate that a reversible and stable redox reaction was achieved on the PTp-COOH nanoparticles.

The structures and morphologies of PTp-COOH were studied after reduction at 0.01 V and subsequent oxidation at 3.0 V by chronoamperometry (Figure 5 and Figure S8 in the Supplementary Information). The FT-IR spectra suggest that the absorption corresponding to the C–C stretching vibration in the aromatic ring and the O–Li stretching vibration increased after the reduction at 0.01 V and then recovered after oxidation at 3.0 V (the white and black arrows, respectively, in Fig. 5a). The results indicate the incorporation of Li^+ with the reduction of the conjugated main chain of PTp-COOH (Fig. 1c). Although the volume changes of the PTp-COOH nanoparticles were observed in the SEM images (Fig. 5b–d), the nanoparticle morphology was maintained after the redox reaction. PTp-COOH nanoparticles approximately 150 nm in size were set on a copper plate (Fig. 5b). The grain boundary was not clearly observed after reduction at 0.01 V (Fig. 5c), but the nanoparticle

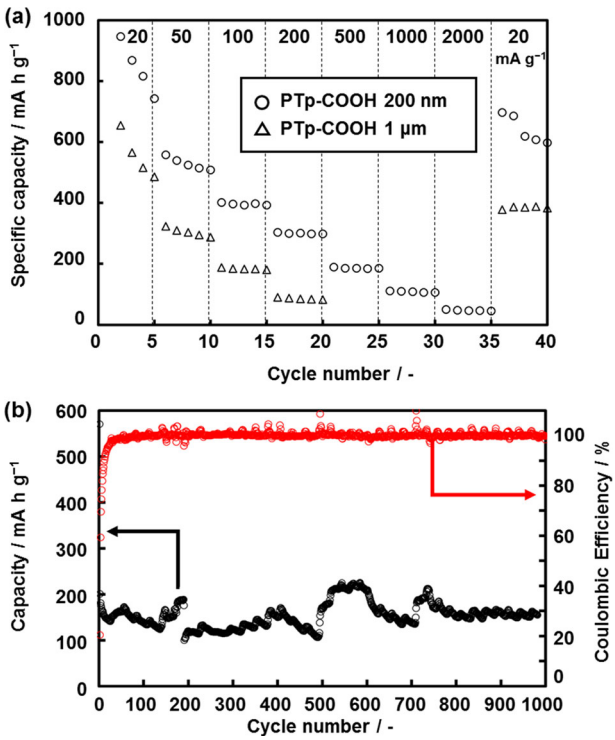

Fig. 4 Cycle stability, rate performance, and particle-size effect of PTp-COOH. a Relationship between the specific capacity and the current density of PTp-COOH nanoparticles approximately 200 nm in size (circles) and microparticles 1 μm in size (triangles). The PTp particles with a larger size have no specific capacity data at a current density higher than 500 mA g^{-1} because the specific capacity of the polymer itself was not observed after subtracting the specific capacity originating from conductive carbon. The specific capacity of the PTp-COOH nanoparticles was reproducible (Figure S6 in the Supplementary Information). The PPy samples showed the same size effect (Figure S7 in the Supplementary Information). **b** Cycle stability and Coulombic efficiency of the PTp-COOH nanoparticles at 200 mAh g^{-1}

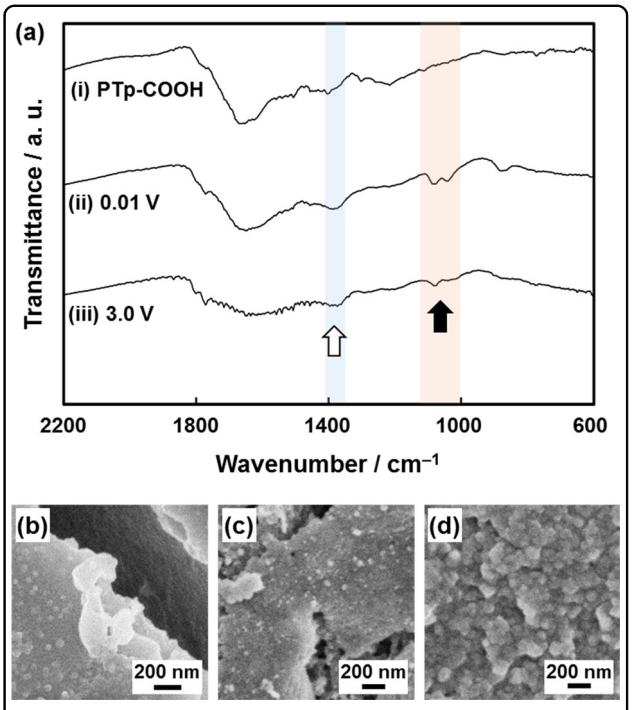

Fig. 5 FT-IR spectra (**a**) and SEM observations (**b**–**d**) of the PTp-COOH nanoparticles after the redox reaction. **a** FT-IR spectra of the PTp-COOH nanoparticles on a copper plate before (i) and after reduction at 0.01 V (ii) and subsequent oxidation at 3.0 V (iii). The absorption bands indicated by the white and black arrows correspond to those of the C–C stretching vibration in the aromatic ring and O–Li stretching vibration, respectively. **b**–**d** SEM images of the PTp-COOH nanoparticles on a copper plate before (**b**) and after reduction at 0.01 V (**c**) and subsequent oxidation at 3.0 V (**d**)

morphology was recovered after oxidation at 3.0 V (Fig. 5d). These volume changes are ascribed to reversible reactions with multiple Li^+ ions.

Discussion

PTp-COOH nanoparticles showed a high performance. The present results suggest that both the molecular structures and morphologies influence the electrochemical properties. In previous works[16,29–38], the electrochemical properties of conductive polymers were not fully studied within 3.0–0.01 V. Since the nanoscale morphologies were not fully controlled, the electrochemical properties of conductive polymers for potential application as anodes have been overlooked in previous works. The advantages of nanostructures have been well studied in active materials based on inorganic compounds[57]. The present work suggests that a similar design strategy can be applied to organic active materials with enhanced electrochemical properties. Nanostructures shorten the diffusion distance of electrons and Li^+ in the active material compared with that in the bulk structure. This effect contributes to improving the specific capacity and rate performance. Since nanostructures lower the influence of the volume changes that occur during redox reactions with multiple Li^+, the cycle stability and rate performance can be improved compared to those of the bulk materials. If the aggregation of the nanostructures is inhibited by the hierarchical morphology design, the effective diffusion pathway of the electrolyte solution is ensured in the electrode. The present results indicate that the morphologies influence the electrochemical properties of organic active materials.

On the basis of the present results, conductive polymers have two types of redox reactions of the heteroaromatic ring with Li^+, such as n doping with Li^+ (Fig. 1b) and further lithium incorporation (Fig. 1c). Moreover, PPy-COOH and PTp-COOH have a carbonyl group for lithium alkoxylation (Fig. 1c). The reaction with Li^+ within 3.0–1.0 V is ascribed to the n doping of the conductive polymers (Fig. 1b)[16,29]. Further reduction of the

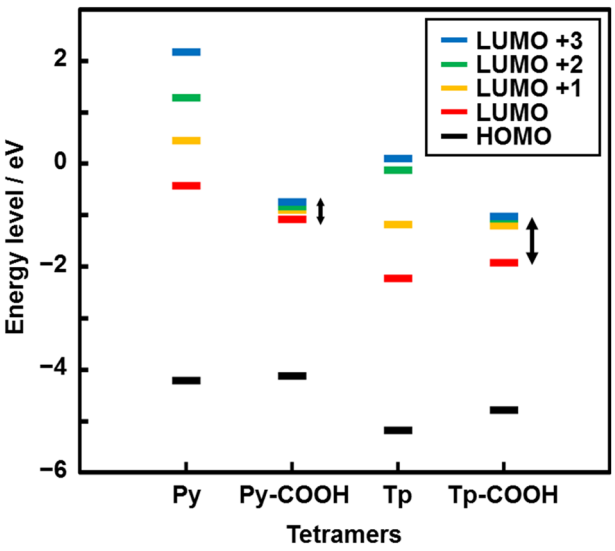

Fig. 6 DFT calculation study of the molecular orbitals near the LUMO and HOMO levels. The energy levels higher than the LUMO are represented by LUMO + 1 (yellow), LUMO + 2 (green), and LUMO + 3 (blue) in ascending order. The arrows indicate the orbitals near the LUMO level that are involved in the enhanced electron acceptability. The energy level was calculated for the tetramers of Py, Py-COOH, Tp, and Tp-COOH by DFT (Table S5 in the Supplementary Information)

conjugated heteroaromatic ring induces the incorporation of Li^+ in the potential range lower than 1.0 V (Fig. 1c). In addition, lithium alkoxylation proceeds with Li^+ on the carbonyl substituent in the conjugated part[41]. If one Li^+ completely reacts with the carbonyl group of PPy-COOH and PTp-COOH, the x increased by 1 compared with the x of PPy and PTp. However, the increment of x with the introduction of the carbonyl group was larger than 1, i.e., 3.03 for PPy-COOH and 4.53 for PTp-COOH, within 3.0–0.01 V. The results indicate that the carboxy groups on the Py and Tp rings promote n doping and lithium incorporation reactions in the conjugated main chain to enhance the specific capacity (Table 1).

The introduction of carboxy groups improves the electron acceptability of PPy-COOH and PTp-COOH. Electron acceptability involves the energy levels of the unoccupied molecular orbitals of these conductive polymers. A previous work showed the correlation between the reduction potential and the energy level of the lowest occupied molecular orbital (LUMO)[58–60]. In the present work, the energy levels of the unoccupied molecular orbitals of the tetramers of Py, Py-COOH, Tp, and Tp-COOH were studied by DFT calculations (Fig. 6 and Table S5 in the Supplementary Information). The introduction of the carboxy groups induced an increase in the number of unoccupied molecular orbitals near the LUMO level (Fig. 6). In other words, the orbitals near the LUMO level were approached in the tetramers of Py-COOH and Tp-COOH (the arrows in Fig. 6). The calculation results imply that the electron acceptability for the reaction with Li^+ is enhanced for PPy-COOH and PTp-COOH. In addition, the lower LUMO level of the Tp-COOH tetramer promotes the introduction of more Li^+ than that of the Py-COOH tetramer (the red lines in Fig. 6). The LUMO level itself and orbitals near the LUMO level are involved in the electron acceptance in the reactions with Li^+. The DFT calculations suggested that a multistage reaction with Li^+ proceeds on the conjugated main chains (Fig. 7). A higher electron density was achieved on the conjugated main chain of the monomer and tetramer (the negative values and orange arrows in Fig. 7). Since the monomer and tetramer showed similar electron-density distributions, similar results can be obtained for polymer states with the elongation of the chain length. These results imply that multiple Li^+ ions, namely, three or four, can be introduced to PTp-COOH. Further study is required to understand the relationship between the functional groups, molecular orbitals, and electrochemical properties. In this way, PPy-COOH and PTp-COOH showed high specific capacities as anodes based on three types of reactions within 3.0–0.01 V. Moreover, molecular design of conductive polymers has the potential to further enhance the specific capacity.

A variety of high-performance anodes based on organic materials has been reported in previous works (Tables S1, S2 and Figure S9 in the Supplementary Information)[41–56]. Although a high specific capacity was reported for organic anodes based on low-molecular-weight compounds (Table S1 in the Supplementary Information)[41–51], their cycle stability was not studied and determined. The polymer-based organic anode possesses cycle stability (Table S2 in the Supplementary Information)[52–56]. The present PTp-COOH nanoparticles showed one of the best performances, including the specific capacity and cycle stability, of the polymer-based organic anodes (Figure S9 in the Supplementary Information). In previous works, further designing the specified molecules and morphologies of polymer-based anodes to enhance the electrochemical properties was not easy. The present work shows the potential of heteroaromatic conductive polymers as high-performance anodes. The design of the molecules and morphologies facilitates a further enhancement of the electrochemical properties.

Conclusions

Conductive-polymer nanostructures, such as PPy-COOH and PTp-COOH, have stable and reversible redox reactions with Li^+ charge and discharge within 3.0–0.01 V vs. Li/Li^+. In particular, the nanostructures play important roles in the enhanced electrochemical properties. The PTp-COOH nanoparticles showed a high specific capacity of 963 mAh g^{-1} with an incorporation of

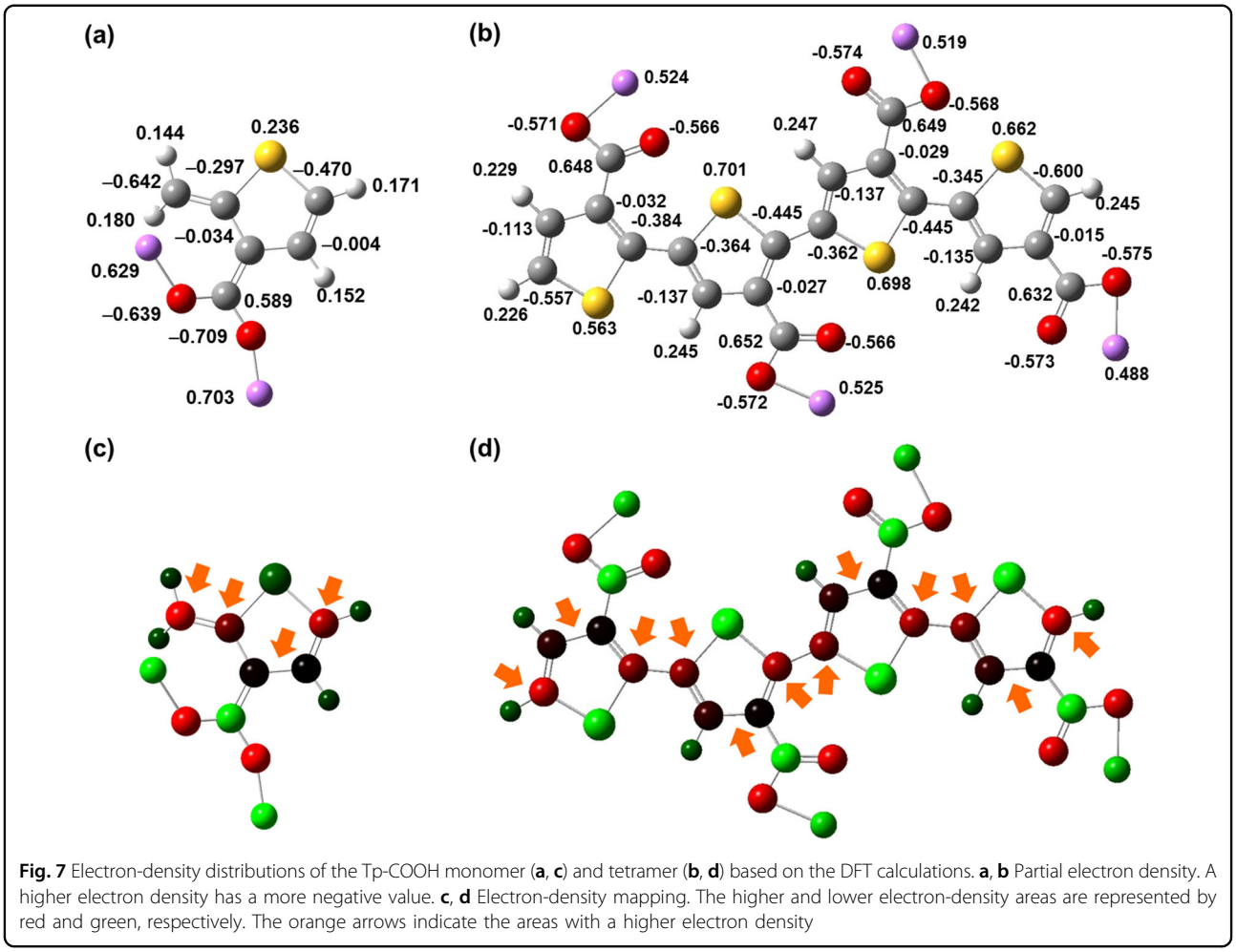

Fig. 7 Electron-density distributions of the Tp-COOH monomer (**a**, **c**) and tetramer (**b**, **d**) based on the DFT calculations. **a**, **b** Partial electron density. A higher electron density has a more negative value. **c**, **d** Electron-density mapping. The higher and lower electron-density areas are represented by red and green, respectively. The orange arrows indicate the areas with a higher electron density

4.53 Li^+ into the monomer at a current density of 20 mA g^{-1}. The high specific capacity is ascribed to multistage redox reactions with Li^+, such as n doping, lithium alkoxylation on the carbonyl group, and lithium incorporation in the heteroaromatic ring. The PTp-COOH nanoparticles showed cycle stability at a higher current density. A decrease in the particle size contributed to an improvement in the specific capacity by shortening the diffusion distance. The PTp-COOH nanoparticles showed a high electrochemical performance combined with a high specific capacity and cycle stability. The present study showed the potential of conductive polymers as lithium-ion battery anodes. Further design of molecules and morphologies will realize high-performance organic charge storage devices based on conductive polymers.

Acknowledgements
This work was partially supported by the Tonen General Research Foundation (to Y.O.) and Sekisui Chemical Nature Research Program (to Y.O.).

Conflict of Interest
The authors declare no competing financial interests.

Supplementary information is available for this paper at https://doi.org/10.1038/s41427-018-0045-2.

Received: 6 January 2018 Revised: 6 March 2018 Accepted: 25 March 2018.
Published online: 17 May 2018

References

1. Etemad, S., Heeger, A. J. & MacDiarmid, A. G. Polyacetylene, $(CH)_x$: the prototype conducting polymer. *Annu. Rev. Phys. Chem.* **33**, 443–469 (1982).
2. Patil, A. O., Heeger, A. J. & Wudl, F. Optical properties of conducting polymers. *Chem. Rev.* **88**, 183–200 (1988).
3. Shirakawa, H. The discovery of polyacetylene film: the dawning of an era of conducting polymers (Nobel Lecture). *Angew. Chem. Int. Ed.* **40**, 2574–2580 (2001).
4. Inzelt, G *Conducting Polymers—A New Era in Electrochemistry* (Springer, Berlin, 2008).
5. Roncali, J. Conjugated poly(thiophenes): synthesis, functionalization, and applications. *Chem. Rev.* **92**, 711–738 (1992).
6. Kirchmeyer, S. & Reuter, K. Scientific importance, properties and growing applications of poly(3,4-ethylenedioxythiophene). *J. Mater. Chem.* **15**, 2077–2088 (2005).

7. Hoeben, F. J., Jonkheijm, P., Meijer, E. W. & Schenning, A. P. H. J. About supramolecular assemblies of π-conjugated systems. *Chem. Rev.* **105**, 1491–1546 (2005).
8. Yoon, H. & Jang, J. Conducting-polymer nanomaterials for high-performance sensor applications: issues and challenges. *Adv. Funct. Mater.* **19**, 1567–1576 (2009).
9. Heinze, J., Frontana-Uribe, B. A. & Ludwings, S. Electrochemistry of conducting polymers—persistent models and new concepts. *Chem. Rev.* **110**, 4724–4771 (2010).
10. Kim, F. S., Ren, G. & Jenekhe, S. A. One-dimensional nanostructures of π-conjugated molecular systems: assembly, properties, and applications from photovoltaics, sensors, and nanophotonics to nanoelectronics. *Chem. Mater.* **23**, 682–732 (2011).
11. Vyas, V. S., Lau, V. W. & Lotsch, B. V. Soft photocatalysis: organic polymers for solar fuel production. *Chem. Mater.* **28**, 5191–5204 (2016).
12. Inagi, S. Fabrication of gradient polymer surfaces using bipolar electrochemistry. *Polym. J.* **48**, 39–44 (2016).
13. Armand, M. B. in *Solid State Batteries* (eds Sequeira, C. A. C. & Hooper, A.) 363 (Martinus Nijhoff Publisher, Dordrecht, 1985).
14. Scrosati, B. Electrochemical properties of conducting polymers. *Prog. Solid State Chem.* **18**, 1–77 (1988).
15. Rudge, A., Davey, J., Raistrick, I. & Gottesfeld, S. Conducting polymers as active materials in electrochemical capacitors. *J. Power Sources* **47**, 89–107 (1994).
16. Novák, P., Müller, K., Santhanam, K. S. V. & Hass, O. Electrochemically active polymers for rechargeable batteries. *Chem. Rev.* **97**, 207–282 (1997).
17. Simon, P. & Gogotsi, Y. Materials for electrochemical capacitors. *Nat. Mater.* **7**, 845–854 (2008).
18. Snook, G., Kao, P. & Best, A. Conducting-polymer-based supercapacitor devices and electrodes. *J. Power Sources* **196**, 1–12 (2011).
19. Song, Z. & Zhou, H. Towards sustainable and versatile energy storage devices: an overview of organic electrode materials. *Energy Environ. Sci.* **6**, 2280–2301 (2013).
20. Muench, S. et al. Polymer-based organic batteries. *Chem. Rev.* **116**, 9438–9484 (2016).
21. Lukatskaya, M. R., Dunn, B. & Gogotsi, Y. Multidimensional materials and device architectures for future hybrid energy storage. *Nat. Commun.* **7**, 12647 (2016).
22. Choi, W., Harada, D., Oyaizu, K. & Nishide, K. Aqueous electrochemistry of poly (vinylanthraquinone) for anode-active materials in high-density and rechargeable polymer/air batteries. *J. Am. Chem. Soc.* **133**, 19839 (2011).
23. Song, Z., Qian, Y., Zhang, T., Otani, M. & Zhou., H. Poly(benzoquinonyl sulfide) as a high-energy organic cathode for rechargeable Li and Na batteries. *Adv. Sci.* **2**, 1500124 (2015).
24. Kuwabara, K., Masaki, H., Imai, H. & Oaki, Y. Substrate coating by conductive polymers through spontaneous oxidation and polymerization. *Nanoscale* **9**, 7895–7900 (2017).
25. Sato, K., Oaki, Y. & Imai, H. Phase separation of composite materials through simultaneous polymerization and crystallization. *NPG Asia Mater.* **9**, e377 (2017).
26. Kuwabara, K., Oaki, Y., Muramatsu, R. & Imai, H. Crystal-surface-induced simultaneous synthesis and hierarchical morphogenesis of conductive polymers. *Chem. Commun.* **51**, 9698–9701 (2015).
27. Sato, K., Oaki, Y. & Imai, H. Incorporation of redox-active guest in conductive and redox-active host: hierarchically structured composite of a conductive polymer and quinone derivative. *Chem. Lett.* **45**, 324–326 (2016).
28. Oaki, Y., Kijima, M. & Imai, H. Synthesis and morphogenesis of organic polymer materials with hierarchical structures in biominerals. *J. Am. Chem. Soc.* **133**, 8594–8599 (2011).
29. Kaner, R. B., MacDiarmid, A. G. & Mammone, R. J. Polyacetylene, $(CH)_x$: an electrode-active material in aqueous and nonaqueous electrolytes. *ACS Symp. Ser.* **242**, 575–584 (1984).
30. Čaja, J., Kaner, R. B. & MacDiarmid, A. G. A rechargeable battery employing a reduced polyacetylene anode and a titanium disulfide cathode. *J. Electrochem. Soc.* **131**, 2744–2750 (2984).
31. Farrington, G. C. & Huq, R. Polyacetylene electrodes for non-aqueous lithium batteries. *J. Power Sources* **14**, 3–9 (1985).
32. Mahammadi, A., Inganäs, O. & Lundström, I. Properties of polypyrrole-electrolyte-polypyrrole cells. *J. Electrochem. Soc.* **133**, 947–949 (1986).
33. Chowdhury, A. N., Harima, Y., Kunugi, K. & Yamashita, K. p- and n-type conductance of electrochemically synthesized poly(3-methyl thiophene) films. *Electrochim. Acta* **41**, 1993–1997 (1996).
34. Bndey, H. L. et al. In situ electron spin resonance study of n- and p-doping of polyterthiophene. *J. Electrochem. Soc.* **142**, 2111–2118 (1995).
35. Arbizzani, C., Catellani, M., Mastragostino, M. & Mingazzini, C. N- and P-doped polydithieno[3,4-B:3′,4′-D] thiophene: a narrow band gap polymer for redox supercapacitors. *Electrochim. Acta* **40**, 1871–1876 (1995).
36. Nawa, M., Nogami, T. & Mikawa, H. Application of activated carbon fiber fabrics to electrodes of rechargeable battery and organic electrolyte capacitor. *J. Electrochem. Soc.* **131**, 1457–1459 (1984).
37. Yata, S., Hato, Y., Sakurai, K. & Osaki, T. Polymer battery employing polyacenic semiconductor. *Synth. Met.* **18**, 645–648 (1987).
38. Yata, S. et al. Studies of porous polyacenic semiconductors toward application III. Characteristics of practical batteries employing polyacenic semiconductive materials as electrodes. *Synth. Met.* **38**, 185–193 (1990).
39. Haupler, B., Wild, A. & Schubert, U. S. Carbonyls: powerful organic materials for secondary batteries. *Adv. Energy Mater.* **5**, 1402034 (2015).
40. Sakaushi, K. & Antonietti, M. Carbon- and nitrogen-based organic frameworks. *Acc. Chem. Rev.* **48**, 1591–1600 (2015).
41. Armand, M. et al. Conjugated dicarboxylate anodes for Li-ion batteries. *Nat. Mater.* **8**, 120–125 (2009).
42. Walker, W. et al. Ethoxycarbonyl-based organic electrode for Li-batteries. *J. Am. Chem. Soc.* **132**, 6517–6523 (2010).
43. Han, X., Qing, G., Sun, J. & Sun, T. How many lithium ions can be inserted onto fused C6 aromatic ring systems? *Angew. Chem. Int. Ed.* **51**, 5147–5151 (2012).
44. Wang, S. et al. Organic $Li_4C_8H_2O_6$ nanosheets for lithium-ion batteries. *Nano Lett.* **13**, 4404–4409 (2013).
45. Fédèle, L., Sauvage, F. & Bécuwe, M. Hyper-conjugated lithium carboxylate based on a perylene unit for high-rate organic lithium-ion batteries. *J. Mater. Chem. A* **2**, 18225–18228 (2014).
46. Mihali, V. A., Renault, S., Nyholm, L. & Brandell, D. Benzenediacrylates as organic battery electrode materials: Na versus Li. *RSC Adv.* **4**, 38004–38011 (2014).
47. Luo, W., Allen, M., Raju, V. & Ji, X. An organic pigment as a high-performance cathode for sodium-ion batteries. *Adv. Energy Mater.* **4**, 1400554 (2014).
48. Wang, C. et al. Extended π-conjugated system for fast-charge and -discharge sodium-ion batteries. *J. Am. Chem. Soc.* **137**, 3124–3130 (2015).
49. Lee, H. H. et al. Mechanistic studies of transition metal-terephthalate coordination complexes upon electrochemical lithiation and delithiation. *Adv. Funct. Mater.* **25**, 4859–4866 (2015).
50. Renault, S. et al. Superlithiation of organic electrode materials: the case of dilithium benzenedipropiolate. *Chem. Mater.* **28**, 1920–1926 (2016).
51. Hu, P., Wang, H., Yang, Y., Lin, J. & Guo, L. Renewable-biomolecule-based bull lithium-ion batteries. *Adv. Mater.* **28**, 3486–3492 (2016).
52. Wu, J. et al. Pushing up lithium storage through nanostructured polyazaacene analogues as anode. *Angew. Chem. Int. Ed.* **54**, 7354–7358 (2014).
53. Wu, J. et al. Nanostructured conjugated ladder polymers for stable and fast lithium storage anodes with high-capacity. *Adv. Energy Mater.* **5**, 1402189 (2015).
54. Liang, Y. et al. Heavily n-dopable π-conjugated redox polymers with ultrafast energy storage capability. *J. Am. Chem. Soc.* **137**, 4956–4959 (2015).
55. Sun, T. et al. A biodegradable polydopamine-derived electrode material for high-capacity and long-life lithium-ion and sodium-ion batteries. *Angew. Chem. Int. Ed.* **55**, 10662–10666 (2016).
56. Xie, J. et al. Novel conjugated ladder-structured oligomer anode with high lithium storage and long cycling capability. *ACS Appl. Mater. Interfaces* **8**, 16932–16938 (2016).
57. Wang, Y., Li, H., He, P., Hosono, E. & Zhou, H. Nano active materials for lithium-ion batteries. *Nanoscale* **2**, 1294–1305 (2010).
58. Araujo, R. B. et al. Designing strategies to tune reduction potential of organic molecules for sustainable high capacity battery application. *J. Mater. Chem. A* **5**, 4430–4454 (2017).
59. Liang, Y., Zhang, P. & Chen, J. Function-oriented design of conjugated carbonyl compound electrodes for high energy lithium batteries. *Chem. Sci.* **4**, 1330–1337 (2013).
60. Kuhn, A., Eschwege, K. Gv & Conradie, J. Reduction potentials of para-substituted nitrobenzenes—an infrared, nuclear magnetic resonance, and density functional theory study. *J. Phys. Org. Chem.* **25**, 58–68 (2012).